

Observation of Hopping and Blockade of Bosons in a Trapped Ion Spin Chain

S. Debnath,^{1,*} N. M. Linke,¹ S.-T. Wang,² C. Figgatt,¹ K. A. Landsman,¹ L.-M. Duan,² and C. Monroe¹

¹*Joint Quantum Institute, Department of Physics,
and Joint Center for Quantum Information and Computer Science,
University of Maryland, College Park, MD 20742, USA*

²*Department of Physics, University of Michigan, Ann Arbor, Michigan 48109, USA*

The local phonon modes in a Coulomb crystal of trapped ions can represent a Hubbard system of coupled bosons. We selectively prepare single excitations at each site and observe free hopping of a boson between sites, mediated by the long-range Coulomb interaction between ions. We then implement phonon blockades on targeted sites by driving a Jaynes-Cummings interaction on individually addressed ions to couple their internal spin to the local phonon mode. The resulting dressed states have energy splittings that can be tuned to suppress phonon hopping into the site. This new experimental approach opens up the possibility of realizing large-scale Hubbard systems from the bottom up with tunable interactions at the single-site level.

Trapped atomic ions are an excellent medium for quantum computation and quantum simulation, acting as a many-body system of spins with programmable and reconfigurable Ising couplings [1–3]. In this system, the long-range spin-spin interaction is mediated by the collective motion of an ion chain and emerges over time scales longer than the propagation time of mechanical waves or phonons through the crystal [4, 5]. On the other hand, at shorter timescales, such a chain represents a bosonic system of phonon modes that describe the local motion of individual ions. Here each local mode is defined by the harmonic confinement of a particular ion with all other ions pinned. In this picture, phonons hop between the local modes due to the long-range Coulomb interaction between ions [6–8]. This intrinsic hopping in trapped ion crystals makes it a viable candidate for simulating many-body systems of bosons [6, 7], boson interference [9] and applications such as boson sampling [10].

Such a system of local oscillators can be approximated to the lowest order of the transverse ion displacement by the phonon Hamiltonian ($\hbar = 1$),

$$H_p = \sum_j (\omega_x + \omega_j) a_j^\dagger a_j + \sum_{j < k} \kappa_{jk} (a_j^\dagger a_k + a_j a_k^\dagger). \quad (1)$$

Here the local mode frequency of each ion is expressed as a sum of the common mode transverse trap frequency ω_x and a position-dependent frequency shift ω_j experienced by the j -th ion [6, 7]. The local mode bosonic creation and annihilation operators are a_j^\dagger and a_j , respectively. The long-range hopping term $\kappa_{jk} = e^2/(2M\omega_x d_{jk}^3)$ is determined by the distance d_{jk} between ions j and k , where e and M are the charge and mass of a single ion.

By applying external controls to the system, on-site interactions between phonons lead to the simulation of Hubbard models of bosons. For instance, applied position-dependent Stark shifts can result in effective phonon-phonon interactions [6]. Combined with phonon hopping between sites, such a system follows the Bose-Hubbard model. In the approach considered here, the

internal spin is coupled to the external phonon mode by driving the spin resonance on a motion-induced sideband transition [11]. This gives rise to nonlinear on-site interactions between spin-phonon excitations (polaritons). Such a system simulates the Jaynes-Cummings-Hubbard model, which describes an array of coupled cavities [7, 8, 12–14].

In order to study the dynamics of such bosonic systems, the local phonon modes must be manipulated and detected faster than the hopping rate. Addressing these modes requires fields that target individual ions in space and each local mode in frequency. Previous experiments have observed hopping only between two sites by either using the collective motion of ions in separate but nearby trapping zones [15, 16] or by varying the spacing between ions in the same trap to spatially resolve each site [17]. In contrast, the direct addressing of each local mode in a single ion crystal circumvents such overheads and provides a complete toolbox for implementing larger bosonic systems by simply increasing the number of ions.

In this Letter, we report the observation of free phonon hopping in an ion chain, and study its suppression by applying targeted phonon blockades on individual sites. We access all local motional modes along the transverse direction of a static linear chain of $^{171}\text{Yb}^+$ ions. Phonons are prepared and measured by driving sideband transitions on each mode faster than the rate of hopping in the chain, with an overall fidelity of 89(2)%. This is achieved by setting the transverse confinement to be much larger than the axial confinement of the chain, which results in suitably low hopping rates due to both a relatively large inter-ion distance ($\sim 10 \mu\text{m}$) and high mass of the $^{171}\text{Yb}^+$ ion.

A phonon blockade is implemented by resonantly driving red-sideband transitions on each site, which couple the internal spin of individually addressed ions to their local phonon mode via a Jaynes-Cummings interaction. In the rotating frame of the free spin and the transverse motional common-mode Hamiltonian ($H_0 = \omega_{HF} \sum_j |e\rangle_j \langle e|_j + \omega_x \sum_j a_j^\dagger a_j$), this interaction is repre-

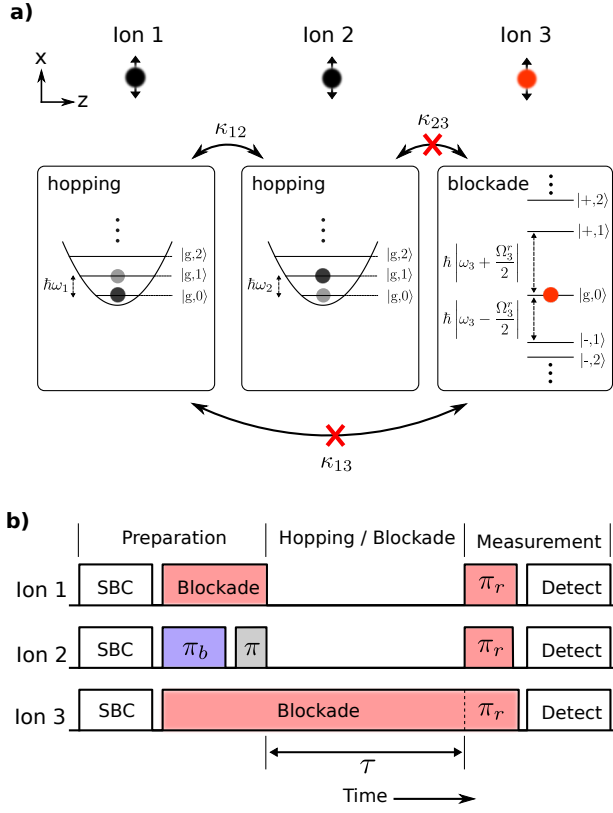


Figure 1. Experimental system for observing hopping of a single phonon excitation between local transverse motional modes along the X-direction. (a) The local phonon frequencies are represented by ω_i in a frame rotating at the transverse common mode frequency ω_x , and κ_{jk} is the phonon hopping strength between modes j and k . Phonon blockades on individual sites (here ion 3) is implemented by driving resonant red sideband transitions with strength Ω_j^r that gives rise to an energy splitting between the ground state $|g,0\rangle$ and the first excited polaritonic states $|\pm,1\rangle$. (b) An experimental sequence where each ion is prepared in the ground state of spin and motion $|g,0\rangle$ using Raman sideband cooling (SBC). A single phonon is excited on ion 2 using π -pulses at the blue sideband (π_b) and carrier (π) transitions. Local phonon blockades are applied using resonant red sideband pulses (shown in red). The hopping duration τ is varied to observe the dynamics of local phonon occupancy (0 or 1 phonon) measured by first projecting it to the internal spin states ($|g\rangle$ or $|e\rangle$) of each ion using red sideband π -pulses (π_r) followed by the detection of state-dependent fluorescence from each ion using a photomultiplier tube array.

sented by the blockade Hamiltonian as

$$H_b = \sum_j \Delta_j |e\rangle_j \langle e|_j + \sum_j \frac{\Omega_j^r}{2} (\sigma_j^+ a_j + \sigma_j^- a_j^\dagger). \quad (2)$$

Here, the spin-1/2 ‘ground’ and ‘excited’ states of the j -th ion are represented by $|g\rangle_j$ and $|e\rangle_j$, respectively, with energy splitting ω_{HF} , and spin raising and lowering operators σ_j^+ and σ_j^- . A local motional red sideband is

driven at a Rabi frequency Ω_j^r and detuned from resonance by Δ_j .

Phonon blockades are applied on individual sites that have ions prepared in the ground state of spin and motion $|g,0\rangle$, where the second index denotes the local mode phonon number. Upon applying the Jaynes-Cummings interaction at resonance ($\Delta_j = 0$), a maximal energy splitting of $|\omega_j \pm \Omega_j^r/2|$ occurs between $|g,0\rangle$ and the next excited polaritonic states $|\pm,1\rangle$. This energy cost suppresses phonons from entering the targeted sites and thereby creates a blockade (see Fig. 1a). This scheme is analogous to implementing photon blockades using single-atom cavity QED systems [18].

The experiment consists of a linear chain of three $^{171}\text{Yb}^+$ ions, each with an internal spin defined by a pair of hyperfine ‘clock’ states as $|g\rangle = |F=0, m_F=0\rangle$ and $|e\rangle = |F=1, m_F=0\rangle$ of the $2S_{1/2}$ electronic ground level with a hyperfine energy splitting of $\omega_{HF} = 2\pi \times 12.642812$ GHz [19]. Here, F and m_F denote the quantum numbers associated with the total atomic angular momentum and its projection along the quantization axis defined by an applied magnetic field of 5.2 G. The external motion of the trapped ions is defined by a linear rf-Paul trap with transverse (X,Y) and axial (Z) harmonic confinement at frequencies $\{\omega_x, \omega_y, \omega_z\} = 2\pi \times \{3.10, 2.85, 0.15\}$ MHz such that the ion chain is aligned along Z with a distance of $d_{j,j+1} = 10.1(2)$ μm between adjacent ions. During an experiment, we excite local phonons in the transverse modes along X, which can then hop between the ion sites. The inherent hopping rates are approximately $\kappa_{j,j+1} \approx 2\pi \times 3$ kHz and $\kappa_{j,j+2} \approx \kappa_{j,j+1}/8$, respectively. The combined effect of the transverse (X) harmonic confinement and repulsion between ions (determined by d_{jk}) define the position-dependent local mode frequency shifts $\{\omega_j\}$. Fig. 1a represents the local modes with frequencies $\{\omega_j\}$ in a frame rotating at the common mode frequency ω_x .

Coherent control of the spin and motion of each ion is implemented with stimulated Raman transitions using a 355 nm mode-locked laser [20], where pairs of Raman beams couple the spin of an ion to its transverse motion [3]. A global beam illuminates the entire chain, and a counterpropagating array of individual addressing beams is focused to a waist of $\approx 1\mu\text{m}$ at each ion. The beat note between the Raman beams can then be tuned to ω_{HF} to implement a ‘carrier’ transition for coherent spin flips, or tuned to $\omega_{HF} \pm (\omega_x + \omega_j)$ to drive a blue- or red-sideband transition involving local phonon modes. The individual addressing beams are modulated independently using a multi-channel acousto-optic modulator [21], each channel of which is driven by a separate arbitrary waveform generator [22]. The wave vector difference $\Delta\vec{k}$ between Raman beams has a projection along both the X and Y directions of motion. Each transverse mode can then be addressed by tuning near their sideband transitions. In order to spectrally resolve each local mode, we choose

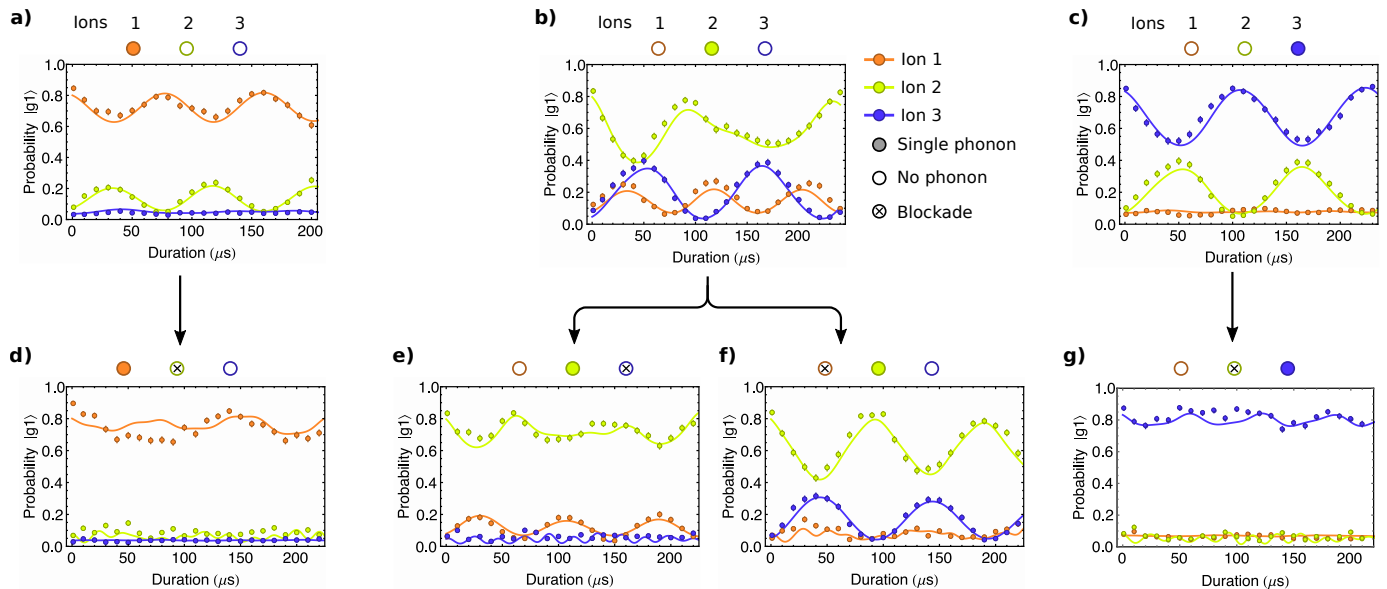


Figure 2. The evolution of local phonon occupancies with initial single-phonon excitations on ions 1, 2, and 3 as shown by the shaded orange, green, and blue circles, respectively. In the absence of a blockade (a-c), the dynamics are governed by the hopping strengths $\{\kappa_{jk}\}$ and the local mode frequencies $\{\omega_j\}$. The corresponding dynamics in the presence of a blockade (d-g) indicate hopping suppression, which is determined by the blockade strength $\{\Omega_j^r\}$. The theoretical plots are obtained by fitting a Jaynes-Cummings Hubbard model (Hamiltonian in Eq. 1 and 2) with free parameters $\{\Omega_j^r\}$, $\{\omega_j\}$ and $\{\kappa_{jk}\}$ using all evolution data sets collectively. Error bars represent statistical uncertainties of 2σ .

sideband Rabi frequencies $\Omega_j^r, \Omega_j^b < |\omega_x - \omega_y|$, while also satisfying $|\omega_j| \ll |\omega_x - \omega_y|$ to prevent crosstalk between the modes.

A typical experimental sequence, as shown in Fig. 1b, starts with the preparation of each ion in state $|g, 0\rangle$ by Doppler cooling and subsequent Raman sideband cooling of each of the transverse modes. A single phonon excitation is introduced at a single site by resonantly driving a blue-sideband and carrier π -pulse to prepare the state $|g, 1\rangle$. In order to minimize the effect of hopping during this process, the sideband and carrier π -pulses are kept short ($\approx 10 \mu\text{s}$ and $\approx 1 \mu\text{s}$, respectively). Phonon blockades are applied to particular ions, initially prepared in the $|g, 0\rangle$ state, by resonantly driving the red-sidebands of their respective local modes. Finally, the single phonon occupancy denoted by states $|g, 0\rangle$ and $|g, 1\rangle$ is measured at each site using a red-sideband π -pulse on each ion, which coherently projects it to spin states $|g\rangle$ and $|e\rangle$, respectively. The spin-dependent fluorescence can then be detected using a multi-channel photomultiplier tube, thereby measuring a binary phonon occupancy of 0 or 1 for each site [3, 19].

Figure 2 shows the hopping dynamics. During free hopping, a single excitation is observed to hop predominantly to the neighboring site. The extent of hopping is indicated by the amplitude of the oscillations in phonon occupancy. This is determined by the strength of hopping κ_{jk} relative to the energy splitting between local modes

Parameter	Fitted value	Measured value
ω_{12}	11.58	—
ω_{23}	7.36	—
κ_{12}	2.90	3.27(19)
κ_{23}	2.96	3.36(20)
Ω_1^r	39.7	43.1(16)
Ω_2^r	45.9	47.6(14)
Ω_3^r	46.3	46.0(19)

Table I. Observed experimental parameters relevant to hopping and the blockade in units of $2\pi \times \text{kHz}$. The values obtained from fits to the hopping data (Fig. 2) are compared with those obtained from direct measurement. The measured hopping rate κ_{ij} is obtained from inter-ion distances $\{d_{12}, d_{23}\} = \{10.1(2), 10.0(2)\} \mu\text{m}$, where the systematic error is due to uncertainty in d_{ij} . The measured red-sideband Rabi frequency is directly obtained from sideband spectroscopy (see Fig.S1). The local mode frequencies measured from sideband spectroscopy are not given due to large Stark shifts that vary between experimental runs with beam alignment [23].

$\omega_{jk} = \omega_j - \omega_k$. We observe different hopping rates between ions 1 and 2 compared to that between 2 and 3, which indicates an asymmetry in the local mode energy differences, $|\omega_{12}| \neq |\omega_{23}|$. This is likely due to a stable non-linearity in the transverse confinement of the ion

trap. We also note that the sign of the local mode energy difference is critical in governing next-nearest neighbor hopping in systems with three or more modes. This is due to a Raman-type hopping process where appropriate energy splittings between the local modes can facilitate hopping between ion 1 and 3 via ion 2 (see supplementary material).

Phonon hopping is also observed in the presence of a blockade applied on neighboring sites (Fig. 2d-g). Here, we resonantly drive on the red sideband, creating a ladder of Jaynes-Cummings eigenstates $\{|g, 0\rangle, |\pm, 1\rangle, |\pm, 2\rangle, \dots\}$, where $|\pm, n\rangle$ is a spin-phonon dressed state with polaritonic excitation number n (Fig. 1a). Since the blockade ion is initially in eigenstate $|g, 0\rangle$, hopping into this site is suppressed when the energy splitting of the first excited states $|\pm, 1\rangle$ is much larger than the hopping rate. This implies that when $|\kappa_{jk}| \ll |\Omega_k^r/2 \pm \omega_{jk}|$, hopping is suppressed from the j -th to k -th site, where the tunable blockade strength is set by the red-sideband Rabi frequency Ω_k^r at the blocked site k . For ions 2 and 3, a higher suppression is observed compared to ions 1 and 2, where the large phonon mode splitting ω_{12} results in some residual hopping despite the applied blockade (see supplementary material).

In Fig. 2, we further observe nonzero phonon occupancies at sites prepared in the motional ground state owing to imperfect initial sideband cooling. Based on the non-oscillatory near-zero phonon occupancies of the hopping data (Fig. 2 a, c, and g for ions 3, 1, and 2, respectively), we estimate average local mode phonon numbers of $\{\bar{n}_1, \bar{n}_2, \bar{n}_3\} = \{0.09, 0.08, 0.04\}$. This also leads to an imperfect preparation and measurement of state $|g, 1\rangle$, which additionally suffers from residual phonon hopping over the finite duration of sideband π -pulses.

We fit the hopping data to a theoretical model using the Hamiltonian presented in Eq. 1 and Eq. 2, with ω_{jk} , κ_{jk} , and Ω_j^r as free parameters. The steady-state phonon occupancy, in the absence of hopping (see Fig. 3), is used to characterize the systematic errors in the preparation and measurement of the states $|g, 0\rangle$ and $|g, 1\rangle$. This is subsequently incorporated into all theoretical curves in Fig. 2 [24] (see supplementary material). The effect of imperfect sideband cooling is directly included by starting from a thermal phonon distribution with mean phonon numbers $\{\bar{n}_j\}$. Both the spin and the motional degrees of freedom are considered in the theoretical simulation of the full hopping dynamics. A single set of parameters (see Table I) is used to fit all data in Fig. 2, which shows a very good agreement between experimental data and the theoretical description of the system. The hopping and blockade strengths given by the parameter values of κ_{jk} and Ω_j^r are consistent with those measured directly from the inter-ion distance and red-sideband spectroscopy, respectively (see supplementary Fig. S1b).

A straightforward way to improve fidelities of local

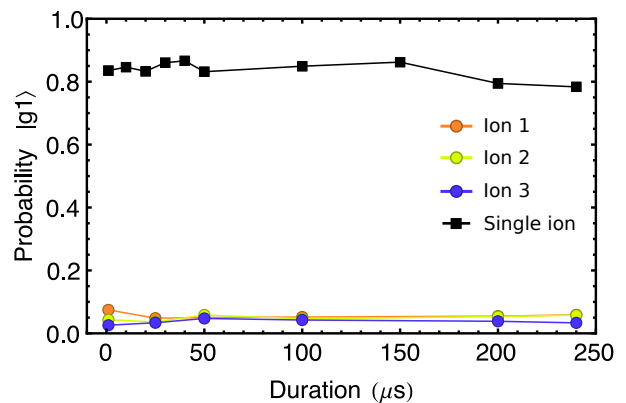


Figure 3. Steady phonon occupancy observed in the absence of hopping when a single ion is prepared in state $|g, 1\rangle$ or in a chain of three ions where each is sideband cooled and prepared in state $|g, 0\rangle$. For the single ion experiment, a constant phonon occupancy indicates negligible crosstalk with other transverse and axial modes of the ion trap. In a three ion chain, the near-zero phonon occupancy indicates that the combined effect of the local mode heating rate and crosstalk with other transverse modes (that are not sideband cooled) is negligible. The duration of both experiments is similar to that used to observe the hopping dynamics in Fig. 2. The probabilities of detecting single phonon excitations in both cases are used to estimate the state preparation and measurement (SPAM) fidelity of states $|g, 0\rangle$ and $|g, 1\rangle$. Error bars showing statistical uncertainties of 2σ are smaller than experimental data points.

phonon operations is setting the sideband Rabi frequency much larger than the hopping strength. In this experiment, since the Raman transition drives both transverse modes, the maximum Rabi frequency is limited by the spacing between the modes ($\omega_x - \omega_y = 2\pi \times 250$) kHz. In future experiments, this can be resolved by rotating the two principle axes of transverse motion (X and Y) with respect to the Raman beams such that only one mode is excited. For multi-phonon hopping experiments, it is also necessary to implement fast measurement of phonon distributions (instead of single phonon occupancy) using cascaded sideband pulses, as has been implemented on single ions [25, 26].

Tunable local phonon blockades can be a useful tool in studying energy transport in ion chains [27]. It can also, in principle, be used in mechanically isolating pairs of ions in a crystal for the implementation of fast entangling gates mediated by their local phonon modes [5, 28].

This work was supported by the ARO with funds from the IARPA LogiQ program, the AFOSR MURI program on Quantum Measurement and Verification, the ARO MURI program on Modular Quantum Circuits, and the NSF Physics Frontier Center at JQI.

- * sdebnath@berkeley.edu
- [1] R. Islam, C. Senko, W. C. Campbell, S. Korenblit, J. Smith, a. Lee, E. E. Edwards, C.-C. J. Wang, J. K. Freericks, and C. Monroe, “Emergence and frustration of magnetism with variable-range interactions in a quantum simulator.,” *Science*, vol. 340, no. 6132, pp. 583–587, 2013.
- [2] T. Monz, D. Nigg, E. A. Martinez, M. F. Brandl, P. Schindler, R. Rines, S. X. Wang, I. L. Chuang, and R. Blatt, “Realization of a scalable Shor algorithm,” *Science (80-.)*, vol. 351, pp. 1068–1070, mar 2016.
- [3] S. Debnath, N. M. Linke, C. Figgatt, K. A. Landsman, K. Wright, and C. Monroe, “Demonstration of a small programmable quantum computer with atomic qubits,” *Nature*, vol. 536, pp. 63–66, aug 2016.
- [4] S.-L. Zhu, C. Monroe, and L.-M. Duan, “Trapped Ion Quantum Computation with Transverse Phonon Modes,” *Phys. Rev. Lett.*, vol. 97, p. 050505, aug 2006.
- [5] S. L. Zhu, C. Monroe, and L. M. Duan, “Arbitrary-speed quantum gates within large ion crystals through minimum control of laser beams,” *Europhys. Lett.*, vol. 73, no. 4, pp. 485–491, 2006.
- [6] D. Porras and J. I. Cirac, “Bose-Einstein Condensation and Strong-Correlation Behavior of Phonons in Ion Traps,” *Phys. Rev. Lett.*, vol. 93, p. 263602, dec 2004.
- [7] P. A. Ivanov, S. S. Ivanov, N. V. Vitanov, A. Mering, M. Fleischhauer, and K. Singer, “Simulation of a quantum phase transition of polaritons with trapped ions,” *Phys. Rev. A*, vol. 80, p. 60301, dec 2009.
- [8] A. Mering, M. Fleischhauer, P. A. Ivanov, and K. Singer, “Analytic approximations to the phase diagram of the Jaynes-Cummings-Hubbard model,” *Phys. Rev. A*, vol. 80, p. 53821, nov 2009.
- [9] K. Toyoda, R. Hiji, A. Noguchi, and S. Urabe, “Hong-Ou-Mandel interference of two phonons in trapped ions,” *Nature*, vol. 527, no. 7576, pp. 74–77, 2015.
- [10] C. Shen, Z. Zhang, and L.-M. Duan, “Scalable Implementation of Boson Sampling with Trapped Ions,” *Phys. Rev. Lett.*, vol. 112, p. 050504, feb 2014.
- [11] D. Leibfried, R. Blatt, C. Monroe, and D. Wineland, “Quantum dynamics of single trapped ions,” *Rev. Mod. Phys.*, vol. 75, pp. 281–324, mar 2003.
- [12] A. D. Greentree, C. Tahan, J. H. Cole, and L. C. L. Hollenberg, “Quantum phase transitions of light,” *Nat. Phys.*, vol. 2, pp. 856–861, dec 2006.
- [13] M. J. Hartmann, F. G. S. L. Brandão, and M. B. Plenio, “Strongly interacting polaritons in coupled arrays of cavities,” *Nat. Phys.*, vol. 2, pp. 849–855, dec 2006.
- [14] K. Toyoda, Y. Matsuno, A. Noguchi, S. Haze, and S. Urabe, “Experimental Realization of a Quantum Phase Transition of Polaritonic Excitations,” *Phys. Rev. Lett.*, vol. 111, p. 160501, oct 2013.
- [15] K. R. Brown, C. Ospelkaus, Y. Colombe, a. C. Wilson, D. Leibfried, and D. J. Wineland, “Coupled quantized mechanical oscillators,” *Nature*, vol. 471, pp. 196–199, mar 2011.
- [16] M. Harlander, R. Lechner, M. Brownnutt, R. Blatt, and W. Hänsel, “Trapped-ion antennae for the transmission of quantum information.,” *Nature*, vol. 471, pp. 200–203, 2011.
- [17] S. Haze, Y. Tateishi, A. Noguchi, K. Toyoda, and S. Urabe, “Observation of phonon hopping in radial vibrational modes of trapped ions,” *Phys. Rev. A*, vol. 85, p. 031401, mar 2012.
- [18] C. Hamsen, K. N. Tolazzi, T. Wilk, and G. Rempe, “Two-Photon Blockade in an Atom-Driven Cavity QED System,” *Phys. Rev. Lett.*, vol. 118, no. 13, pp. 1–6, 2017.
- [19] S. Olmschenk, K. C. Younge, D. L. Moehring, D. N. Matsukevich, P. Maunz, and C. Monroe, “Manipulation and detection of a trapped Yb+ hyperfine qubit,” *Phys. Rev. A*, vol. 76, p. 052314, nov 2007.
- [20] D. Hayes, D. N. Matsukevich, P. Maunz, D. Hucul, Q. Quraishi, S. Olmschenk, W. Campbell, J. Mizrahi, C. Senko, and C. Monroe, “Entanglement of atomic qubits using an optical frequency comb,” *Phys. Rev. Lett.*, vol. 104, no. 14, pp. 1–4, 2010.
- [21] Model H-601 Series 32-Channel UV Acousto-Optic Modulator, PN: 66948-226460-G01, Harris Corporation.
- [22] Model WX1284C-1 1.25 GS/s Four Channel Arbitrary Waveform Generator, PN: 126182, Tabor Electronics Ltd.
- [23] A. C. Lee, J. Smith, P. Richerme, B. Neyenhuis, P. W. Hess, J. Zhang, and C. Monroe, “Engineering large Stark shifts for control of individual clock state qubits,” *Phys. Rev. A*, vol. 94, p. 042308, oct 2016.
- [24] C. Shen and L.-M. Duan, “Correcting detection errors in quantum state engineering through data processing,” *New J. Phys.*, vol. 14, p. 053053, may 2012.
- [25] S. An, J.-N. Zhang, M. Um, D. Lv, Y. Lu, J. Zhang, Z.-Q. Yin, H. T. Quan, and K. Kim, “Experimental test of the quantum Jarzynski equality with a trapped-ion system,” *Nat. Phys.*, vol. 11, no. 2, pp. 193–199, 2014.
- [26] M. Um, J. Zhang, D. Lv, Y. Lu, S. An, J.-N. Zhang, H. Nha, M. S. Kim, and K. Kim, “Phonon arithmetic in a trapped ion system,” *Nat. Commun.*, vol. 7, p. 11410, apr 2016.
- [27] M. Ramm, T. Pruttivarasin, and H. Häffner, “Energy transport in trapped ion chains,” *New J. Phys.*, vol. 16, p. 063062, jun 2014.
- [28] J. D. Wong-Campos, S. A. Moses, K. G. Johnson, and C. Monroe, “Demonstration of two-atom entanglement with ultrafast optical pulses,” *Arxiv 1709.05179*, sep 2017.
- [29] K. G. Johnson, J. D. Wong-Campos, A. Restelli, K. A. Landsman, B. Neyenhuis, J. Mizrahi, and C. Monroe, “Active stabilization of ion trap radiofrequency potentials,” *Rev. Sci. Instrum.*, vol. 87, no. 5, p. 053110, 2016.

SUPPLEMENTARY MATERIALS

1. Spectroscopy of Local Phonon Modes.

Figure S1 shows the spectroscopy of the motional sidebands of local modes of each ion in a chain of three. The blue sideband spectrum (Fig.S1a) shows the two transverse motional modes of each ion separated by $\omega_x - \omega_y = 2\pi \times 250$ kHz. We choose to excite the X -mode, which has the higher mode frequency. The red sideband spectrum is obtained by preparing each ion in the $|g, 1\rangle$ state with a single phonon excited in the X -mode followed by a red sideband π -pulse and fluorescence detection

(Fig.S1b). The red sideband Rabi frequencies Ω_j^r of the local modes are extracted from the spectroscopy and are shown in Table I.

The transverse common mode trap frequencies (ω_x, ω_y) are set by the amplitude of the ion trap rf signal. This can drift over time causing the local mode frequencies to vary. Therefore, in order to mitigate errors in the spectral addressing of each local mode, the transverse confinement (ω_x) is actively stabilized [29].

2. State Preparation and Measurement (SPAM) Error Correction.

In the experiment, the state preparation and measurement are not perfect, due to single ion fluorescence detection error, imperfect cooling ($\bar{n} > 0$), and mapping of phonon occupancy. For detection, the phonon number states $|0\rangle$ and $|1\rangle$ are mapped onto the spin states $|g\rangle$ and $|e\rangle$ respectively.

We consider two separate single-ion SPAM errors, ϵ_g for $|g\rangle$ and ϵ_e for $|e\rangle$. In order to determine these, we prepare the ion in state $|g\rangle$ and $|e\rangle$ and measure the fraction of bright events. Our readout errors are $\epsilon_g = 0.26\%$ and $\epsilon_e = 0.91\%$. The experimental readout $P_g = 1 - P_e$ and P_e are then related to theoretical predictions by [24]

$$\begin{pmatrix} P_g \\ P_e \end{pmatrix} = \begin{pmatrix} 1 - \epsilon_g & \epsilon_e \\ \epsilon_g & 1 - \epsilon_e \end{pmatrix} \begin{pmatrix} P_g^{\text{th}} \\ P_e^{\text{th}} \end{pmatrix}. \quad (\text{S1})$$

We now include the effect of imperfect cooling. After sideband cooling, the phonon distribution is assumed to be thermal with an average phonon number of \bar{n} . Then, we can consider the initial state to be an incoherent mixture of different phonon numbers, with probabilities $P_n = \bar{n}^n / (\bar{n} + 1)^{n+1}$. Hence, the effect of imperfect cooling can be directly incorporated in the theoretical model.

Finally, we extend the error model to include another layer of SPAM error in the detection of phonon occupancy due to imperfect mapping to spin states with errors ϵ'_g and ϵ'_e . Assuming the ground state preparation is limited only by fluorescence detection error and the effect of the thermal phonon distribution ($\bar{n} > 0$), i.e., $\epsilon'_g = 0$, we have

$$\begin{pmatrix} P_g \\ P_e \end{pmatrix} = \begin{pmatrix} 1 - \epsilon_g & \epsilon_e \\ \epsilon_g & 1 - \epsilon_e \end{pmatrix} \begin{pmatrix} 1 & \epsilon'_e \\ 0 & 1 - \epsilon'_e \end{pmatrix} \begin{pmatrix} P_g^{\text{th}}(\bar{n}) \\ P_e^{\text{th}}(\bar{n}) \end{pmatrix}, \quad (\text{S2})$$

where the theoretical values $P_g^{\text{th}}(\bar{n})$ and $P_e^{\text{th}}(\bar{n})$ depend on the mean phonon number \bar{n} . From Fig. 3 of the main text, the experimentally-measured probabilities are $P_e \approx 0.836$ and $P_e \approx 0.048$ for the state $|g, 1\rangle$ and $|g, 0\rangle$, respectively (averaged over time and ions). Fitting the theoretical values to those, we have two variables, \bar{n} and ϵ'_e , and two equations, from which we can extract the values as $\bar{n} \approx 0.055$ and $\epsilon'_e \approx 0.114$. The SPAM error

matrix is

$$M_{\text{SPAM}} = \begin{pmatrix} 1 - \epsilon_g & \epsilon_e \\ \epsilon_g & 1 - \epsilon_e \end{pmatrix} \begin{pmatrix} 1 & \epsilon'_e \\ 0 & 1 - \epsilon'_e \end{pmatrix} \quad (\text{S3})$$

$$\approx \begin{pmatrix} 0.997 & 0.122 \\ 0.003 & 0.878 \end{pmatrix},$$

which is then used to scale all theoretical curves.

3. Long-range Hopping and Raman-like Hopping.

The phonon hopping amplitude κ_{ij} decays as $1/d_{ij}^3$, where d_{ij} is the distance between ions i and j , so direct long-range hopping $\kappa_{13} \approx \kappa_{12}/8$. Hence, we expect the effect of long-range hopping in the three ion chain to be unimportant. A natural approach is to use the Rabi flopping of the free hopping data in Fig.2a of the main text to extract the local mode energy difference ω_{12} and κ_{12} . Similarly, ω_{23} and κ_{23} are expected to be extracted in the same way from Fig.2c. However, this picture of two-site (two-level) approximation is incomplete, primarily due to a Raman-like process of hopping, i.e., phonons hopping from ion 1 to ion 2 and then from ion 2 to ion 3. We have confirmed our observation by using the two-ion approximation to extract out the experimental parameters; the fitted parameters deviate substantially from those in Table I of the main text and the former produce poor fits to other panels of data.

In addition, the relative sign between ω_{12} and ω_{23} does not matter in the two-ion picture. However, considering the dynamics of the full system of three modes, the relative sign is important. One can again understand why this is the case via an analogy to a Raman process. Phonons can hop from ion 1 to ion 3 via ion 2. If ω_{12} and ω_{23} had opposite signs, the magnitude of ω_{13} would be much smaller (analogous to the two-photon detuning in Raman transitions). This would lead to a Raman-like hopping from ion 1 to 3, which would induce much stronger oscillations than are observed in the experiment.

Therefore, we need to consider phonon hopping among three ions to correctly model their full dynamics. In the theoretical fitting, we use seven free parameters $\omega_{12}, \omega_{23}, \kappa_{12}, \kappa_{23}, \Omega_1^r, \Omega_2^r, \Omega_3^r$ to fit all experimental data in Fig.2 of the main text, taking into account the SPAM error and the thermal phonon distribution after sideband cooling.

4. Additional Explanation on the Phonon Blockade Data.

This section provides some additional explanation on a few non-intuitive behaviors of the blockade data. To un-

derstand it better, we include a simplified three-level picture. Consider Fig. 2d of the main text. Three collective states are predominantly involved: $|g, 1\rangle_1|g, 0\rangle_2|g, 0\rangle_3$, $|g, 0\rangle_1|g, 1\rangle_2|g, 0\rangle_3$, and $|g, 0\rangle_1|e, 0\rangle_2|g, 0\rangle_3$, where the subscript labels the ion number. In this subspace, the Hamiltonian can be approximated as

$$H = \begin{pmatrix} 0 & \kappa_{12} & 0 \\ \kappa_{12} & -\omega_{12} & \Omega_2^r/2 \\ 0 & \Omega_2^r/2 & -\omega_{12} \end{pmatrix}, \quad (\text{S4})$$

where $\kappa_{12}/2\pi \approx 2.9$ kHz, $\omega_{12}/2\pi \approx 11.58$ kHz, and $\Omega_2^r \approx 45.9$ kHz (the common energy ω_1 is subtracted out). Instead of suppressing hopping, the local mode frequency difference ω_{12} facilitates hopping due to the fact that it partially offsets the blockade strength $\Omega_2^r/2$. Figures S2a and S2b compare the scenarios in which $\omega_{12}/2\pi = 11.58$ kHz and $\omega_{12}/2\pi = 0$ kHz, respectively. It is evident that hopping is further suppressed for the case $\omega_{12}/2\pi = 0$ kHz. Since $|\omega_{12}| > |\omega_{23}|$, this explains why the blockade data in Fig. 2d seems to have stronger

oscillation than that in Fig. 2g. In addition, from Fig. S2, we also see that much of the state population is stored in $|g, 0\rangle_1|e, 0\rangle_2|g, 0\rangle_3$, which explains the observation that, for Fig. 2d, ion 1 seems to have a stronger oscillation than ion 2; the apparent non-conservation of the total phonon numbers is due to our detection method of mapping phonons to spins via a single red sideband pulse.

In addition, we can understand how the red sideband Rabi frequencies come into play for the blockade data. For the free hopping data, red sideband Rabi frequency does not play a role other than some small hopping during the short pulse period. So the free hopping data (Fig. 2a-c) is not sensitive to $\Omega_1^r, \Omega_2^r, \Omega_3^r$. However, for the blockade data (Fig. 2d-g), due to a much longer hopping period and the offset between local mode frequency difference and the blockade strength, the observations depend sensitively on $\Omega_1^r, \Omega_2^r, \Omega_3^r$. Therefore, we also fit the red sideband blockade strengths as free parameters in the theoretical model.

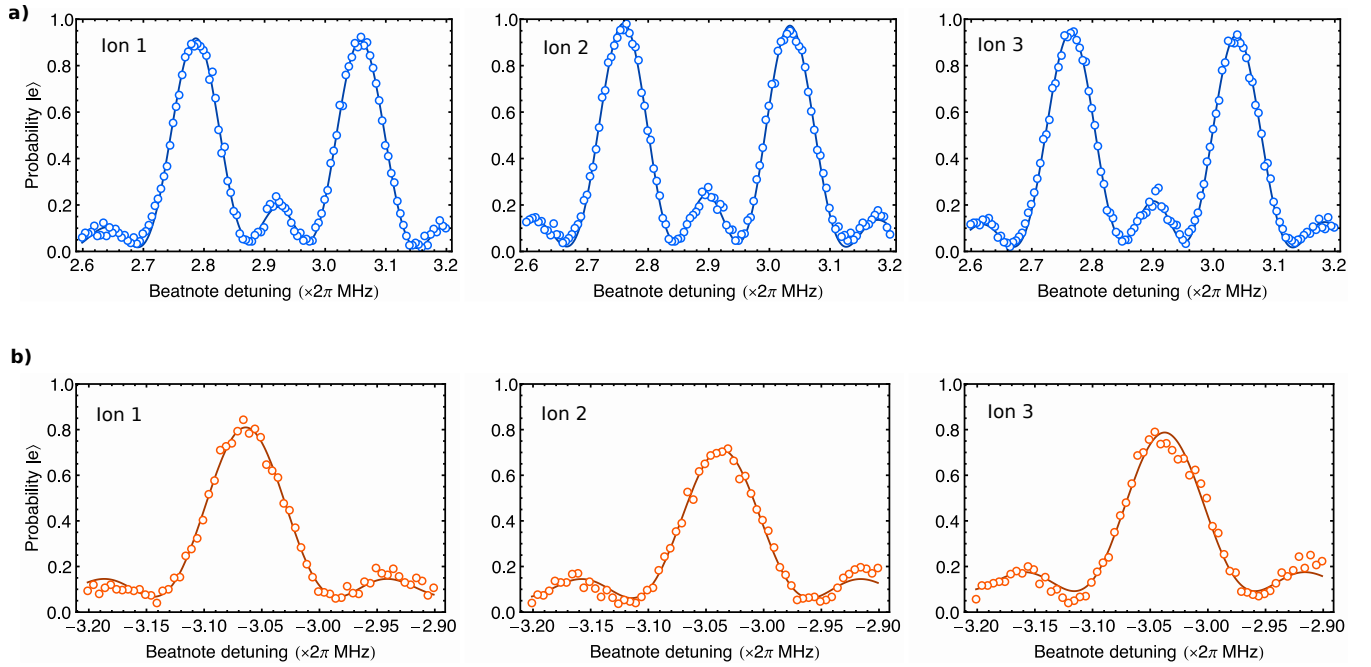


Figure S1. Sideband spectroscopy of local phonon modes. (a) The blue sideband spectroscopy showing sideband transitions for the two transverse local modes of each ion in a chain of three. Each ion is Raman sideband-cooled to the motional ground state of both modes. A blue sideband π -pulse is then applied on each ion, which changes its state from $|g, 0\rangle$ to $|e, 1\rangle$ when resonant with a sideband transition. The two transverse local modes are sufficiently separated by ≈ 250 kHz compared to the sideband transition strength such that the mode with higher energy can be spectrally addressed for introducing local phonon excitations during the ‘preparation’ step of an experimental sequence as shown in Fig. 1b. (b) Red sideband spectroscopy of the higher energy transverse local mode. Each ion is initialized to $|g, 1\rangle$ as shown in Fig. 1b followed by a red sideband π -pulse that flips the state from $|g, 1\rangle$ to $|e, 0\rangle$ followed by measurement of the spin-up state $|e\rangle$ using state-dependent fluorescence. The red sideband Rabi frequencies obtained by fitting the data determines the strength of phonon blockade applied on each ion (see Fig. 1a).

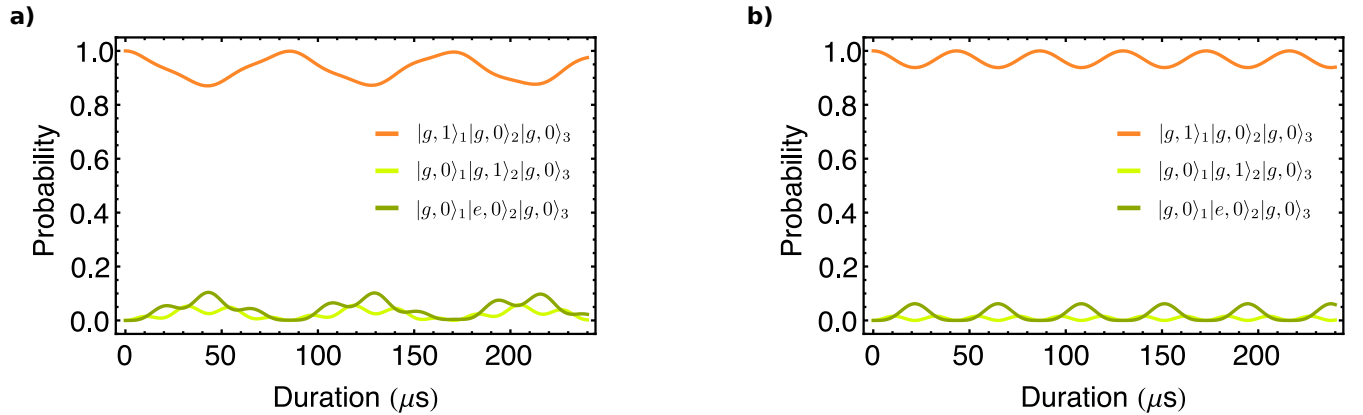


Figure S2. A theoretical analysis of the effect of phonon blockade on ion 2 when an initial phonon excitation is introduced on ion 1. The analysis captures phonon hopping in terms of the time evolution of the states $|g, 1\rangle_1|g, 0\rangle_2|g, 0\rangle_3$, $|g, 0\rangle_1|g, 1\rangle_2|g, 0\rangle_3$, and $|g, 0\rangle_1|e, 0\rangle_2|g, 0\rangle_3$, which are predominantly coupled to each other via the hopping and blockade interactions. (a) Shows the dynamics for real experimental conditions where $\omega_{12}/2\pi = 11.58$ kHz. This simulates experimental data in Fig. 2d. (b) Shows the dynamics for the case where $\omega_{12}/2\pi = 0$ kHz which exhibits a higher suppression of hopping.